Pathways to Highly Oxidized Products in the Delta 3-Carene + OH System

D'Ambro, Emma L.

2022-02-15

D'Ambro , E L , Hyttinen , N , Moller , K H , Iyer , S , Otkjaer , R , Bell , D M , Liu , J , Lopez-Hilfiker , F D , Schobesberger , S , Shilling , J E , Zelenyuk , A , Kjaergaard , H G , Thornton , J A & Kurten , T 2022 , ' Pathways to Highly Oxidized Products in the Delta 3-Carene + OH System ' , Environmental Science & Technology , vol. 56 , no. 4 , pp. 2213-2224 . https://doi.org/10.1021/acs.est.1c06949

http://hdl.handle.net/10138/354124
https://doi.org/10.1021/acs.est.1c06949

unspecified
acceptedVersion

Pathways to highly oxidized products in the Δ3-carene + OH system

Emma L. D'Ambro[1,2,!], Noora Hyttinen[2,3,@], Kristian H. Møller[4], Siddharth Iyer[2,3,#], Rasmus V. Otkjær[4], David M. Bell[5,$], Jiumeng Liu[5,%], Felipe D. Lopez-Hilfiker[6,^], Siegfried Schobesberger[6,&], John E. Shilling[5], Alla Zelenyuk[5], Henrik G. Kjaergaard[4], Joel A. Thornton[1,6*], Theo Kurtén[2,3*]*

[1]Department of Chemistry, University of Washington, Seattle, WA, 98195, USA
[2]Department of Chemistry, University of Helsinki, Helsinki, FI-00100, Finland
[3] Institute for Atmospheric and Earth System Research (INAR), University of Helsinki, Helsinki, FI-00100, Finland
[4]Department of Chemistry, University of Copenhagen, Copenhagen, DK-2100, Denmark
[5]Atmospheric Sciences and Global Change Division, Pacific Northwest National Laboratory, Richland, WA, 99354, USA
[6]Department of Atmospheric Sciences, University of Washington, Seattle, WA, 98195 USA

Author Information

Corresponding Authors

[*]Email: dambro.emma@epa.gov
[*]Email: thornton@atmos.uw.edu
[*]Email: theo.kurten@helsinki.fi

Abstract

Oxidation of the monoterpene Δ3-carene ($C_{10}H_{16}$) is a potentially important and under-studied source of atmospheric secondary organic aerosol (SOA). We present chamber-based measurements of the speciated gas and particle phases during photochemical oxidation of Δ3-carene. We find evidence of highly oxidized organic molecules (HOM) in the gas phase and relatively low volatility SOA dominated by C_7-C_{10} species. We then use computational methods to develop the first stages of a Δ3-carene photochemical oxidation mechanism and explain some of our measured compositions. We find that alkoxy bond scission of the cyclohexyl ring likely leads to efficient HOM formation, in line with previous studies. We also find a surprising role for the abstraction of primary hydrogens from methyl groups, which has been calculated to be rapid in the α-pinene system, and suggest more research is required to determine if this is more general to other systems and a feature of autoxidation. This work develops a more comprehensive view of Δ3-carene photochemical oxidation products via measurements and lays out a suggested mechanism of oxidation via computationally derived rate coefficients.

Keywords

Atmospheric chemistry, Autoxidation, Highly Oxidized Organic Molecules (HOM), Monoterpene oxidation, Secondary Organic Aerosol (SOA)

Synopsis

Laboratory experiments and rate calculations are synthesized to develop a photochemical oxidation mechanism for Δ3-carene, which may be an important precursor for secondary organic aerosol.

1 Introduction

Secondary organic aerosol (SOA), particulate matter that is formed in the atmosphere as opposed to being directly emitted, is a substantial component of submicron aerosols[1, 2] which are particularly detrimental to human health and are the source of much of the uncertainty related to aerosol-climate effects[3]. One of the largest sources of SOA is the oxidation of biogenic volatile organic compounds (BVOC)[4] that are emitted from vegetation and have lifetimes of hours or less against atmospheric oxidation. Monoterpenes ($C_{10}H_{16}$), one class of BVOC, play a well-documented role in SOA formation and growth.

To understand and predict SOA formation and growth, mechanisms of BVOC conversion to lower volatility compounds are required. One mechanism that has recently garnered much attention is autoxidation[5]. In the context of atmospheric gas-phase chemistry, autoxidation involves an organic peroxy (RO_2) or alkoxy (RO) radical abstracting a hydrogen from elsewhere in the molecule, followed by O_2 addition. Multiple unimolecular steps can rapidly increase the oxygen content of a molecule, while keeping the carbon backbone mostly intact[6]. Autoxidation is thus a pathway to form highly-oxygenated organic molecules (HOM), which are defined to have six or more oxygens[6]. Most studies on HOM formation and identification have focused on α-pinene which is considered the most abundant monoterpene[7]. Yet, even for the α-pinene ozonolysis system, a molecular-level mechanism for HOM formation was only proposed recently[8]. Due to the often very low volatility of HOM, they can impact SOA formation even when formed in low yields, thus exploring the possibility of other BVOC to form HOM is important.

One intriguing monoterpene in this regard is Δ3-carene. Δ3-carene is predicted to have lower emission rates than α-pinene globally[7], although regionally they have been measured in roughly equivalent concentrations[9]. Additionally, Δ3-carene has a larger OH reaction rate constant (8.0×10^{-11} cm^3 $molec^{-1}$ s^{-1})[10] than α-pinene (5.4×10^{-11} cm^3 $molec^{-1}$ s^{-1})[11]. Taken together, in certain environments such as the boreal forest, OH can react with Δ3-carene as often as α-pinene, suggesting that the production rate of HOM from Δ3-carene photochemical oxidation could be as large as that of α-pinene in these environments, depending on the HOM yields.

Despite the potential importance of Δ3-carene, little is known about its oxidation initiated by OH radicals. Previous Δ3-carene photochemical oxidation studies determined the presence and yield of caronaldehyde (14-77%), a primary first-generation product[10, 12-15], and an SOA yield of 1.6-40%[16-19]. However, only one study was carried out in the absence of NO_x[14] and all of the studies used elevated levels of precursors (Δ3-carene, and NO_x when used), suggesting they likely enhanced the role of bimolecular reactions of radicals over autoxidation compared to the atmosphere[20]. More recently, 13 compounds with molecular formulas of $C_{8\text{-}10}H_{12\text{-}16}O_{1\text{-}4}$ were detected in the particle phase, with structures assigned to the formulae based on a combination of literature and speculation[21].

We present herein a combined chamber and theoretical study of the OH oxidation of Δ3-carene. We investigate the gas and particle phase products of this reaction produced in a steady-state chamber experiment and use known gas-phase organic chemistry to predict possible products matching the molecular formulas we observe. We use quantum chemical calculations to calculate the rate coefficients of various peroxy and alkoxy H-shifts and bond scission/ring opening reactions to predict the most likely unimolecular reactions potentially leading to HOM formation. We find that alkoxy bond scission of the cyclohexyl ring is the most likely pathway to HOM formation and develop a mechanism for the first steps of Δ3-carene photochemical oxidation.

2 Methods

2.1 Laboratory Experiments

Experiments were performed in the Pacific Northwest National Laboratory (PNNL) environmental chamber[22] in 2015 as part of the Secondary Organic Aerosol From Forest Emissions Experiment (SOAFFEE), which has been described previously[20, 23, 24]. The PNNL chamber is 10.6 m^3 and was operated in continuous-flow mode with a total flow of 48.2 L min^{-1}, resulting in a chamber lifetime of ~3.7 hours. (1S)-(+)-3-carene (90% purity, Sigma-Aldrich, from here on written as Δ3-carene) was passed into the chamber to maintain a steady state concentration of 10 ppb before lights were switched on to initiate photochemistry. H_2O_2 was injected via an automated syringe as a radical OH and HO_2 precursor, at a mixing ratio of 1 ppm H_2O_2 before photochemistry was initiated. Quasi-monodisperse 50 nm solid ammonium sulfate seed particles were continually added. The chamber was operated at room temperature and 50% RH.

A suite of online gas and particle phase instruments were employed to characterize the chemical speciation and concentration within the chamber. Ozone (Thermo Environmental Instruments model 49C), $NO/NO_2/NO_x$ (Thermo Environmental Instruments model 42C), and Δ3-carene (Proton-transfer-reaction mass spectrometer, Ionicon) concentrations were monitored. Mass loading and bulk submicron particle-phase composition were measured with an Aerodyne high-resolution time-of-flight aerosol mass spectrometer. The chemically speciated gas- and particle-phase composition of semi- and low-volatility compounds[25] in near-real time were measured with a high resolution time-of-flight chemical ionization mass spectrometer (HR-ToF-CIMS) with iodide ionization coupled to a Filter Inlet for Gases and AEROsols (FIGAERO)[26]. We do not convert signal to concentration for the HR-ToF-CIMS, but use the measurements to qualitatively compare compositions and as a basis for building oxidation mechanisms. The operation of the FIGAERO-CIMS has been described previously[23]. Briefly, the FIGAERO was operated in a cycle with a 43 min aerosol collection and simultaneous real-time gas phase measurements, followed by a 70 min thermal desorption with a temperature ramp from room temperature to 200 °C at a rate of 10 °C min^{-1}, followed by a 10 min cool down to room temperature. Gas phase zeros were performed by overblowing the pinhole with ultra high purity N_2 every 5 min, and particle phase blanks were obtained by inserting a secondary filter upstream from the primary collection filter every 4^{th} collection.

In addition, the volatility of size-selected SOA particles was measured using a single particle mass spectrometer, miniSPLAT, described in detail elsewhere[27]. Briefly, SOA particles from the PNNL chamber were extracted, size selected with a differential mobility analyzer, passed through two charcoal denuders to remove gas-phase organics, and loaded into a stainless-steel evaporation chamber that was partially filled with activated carbon to continuously remove evaporated organics. The miniSPLAT was used to periodically sample particles from the evaporation chamber to characterize changes in their vacuum aerodynamic diameter and mass spectra. Room-temperature evaporation kinetics of the size-selected SOA particles, expressed as organic volume fraction remaining (VFR) as a function of evaporation time, was quantified by measuring change in particle vacuum aerodynamic diameter with 0.5% precision, accounting for the volume of the inorganic seed.

2.2 Quantum Chemical Rate Calculations

Rate coefficient calculations were performed according to the approach in Møller et al.[28], based on multiconformer transition-state theory (MC-TST)[29] and presented numerous times before (e.g.[30-34]). Briefly, the calculations included six steps. (1) A systematic conformer search

was performed for the reactants, products, and transition states in Spartan '16[35] with the MMFF force field. The FFHINT keyword was utilized to enforce a neutral charge on the radical center and constraints were applied to selected bond lengths for the transition states. (2) All identified structures were optimized at B3LYP/6-31+G(d) level of theory in Gaussian 09[36] or 16[37]. (3) Unique structures, determined by energy and dipole moment (differences > 1×10^{-5} H and > 1.5×10^{-2} D)[38], within 2 kcal mol^{-1} in electronic energy of the lowest energy conformer were then optimized at the ωB97X-D/aug-cc-pVTZ level. Additionally, harmonic vibrational frequencies were calculated to obtain zero-point corrected energies of all species and to confirm the character of the optimized transition state structures with a single imaginary frequency corresponding to the H-shift or bond scission. (4) To obtain a more accurate barrier height, ROHF-ROCCSD(T)-F12a/cc-pVDZ-F12 single-point energy calculations (denoted "F12" for simplicity from here on) were then performed using Molpro 2015.1[39] on the lowest energy ωB97X-D/aug-cc-pVTZ optimized reactant, product, and transition state conformers for selected reactions of the first generation alkoxy (Scheme 1, *M3*). Exclusion of F12 singe-point calculations results in a factor of ~2 average difference in rate coefficients and increases their uncertainty to about two orders of magnitude[40]. (5) Finally, the Eckart tunneling coefficient[41] was calculated using the forward and reverse barrier heights (energy differences at the ωB97X-D/aug-cc-pVTZ level, or at the F12 level where available) between the lowest-energy transition state and the reactant and product conformers connected to it via intrinsic reaction coordinate (IRC) paths at the B3LYP/6-31+G(d) level. The tunneling coefficient calculation also included the imaginary frequency of the transition state at the ωB97X-D/aug-cc-pVTZ level calculated in step 3. (6) Rate coefficients were calculated using MC-TST with the Eckart tunneling coefficients, ωB97X-D/aug-cc-pVTZ partition functions, relative energies between conformers and zero-point vibrational corrections and electronic energies for the barrier height calculated at either the ωB97X-D/aug-cc-pVTZ or, where available, F12 levels. The pressure dependence of RO_2 H-shift reactions has been shown to be negligible in the α-pinene ozonolysis system[42] at 298 K and 1 atm, and thus was not studied here, as similar results are expected for our reactions.

3 Results & Discussion

3.1 Δ3-carene photochemical oxidation products

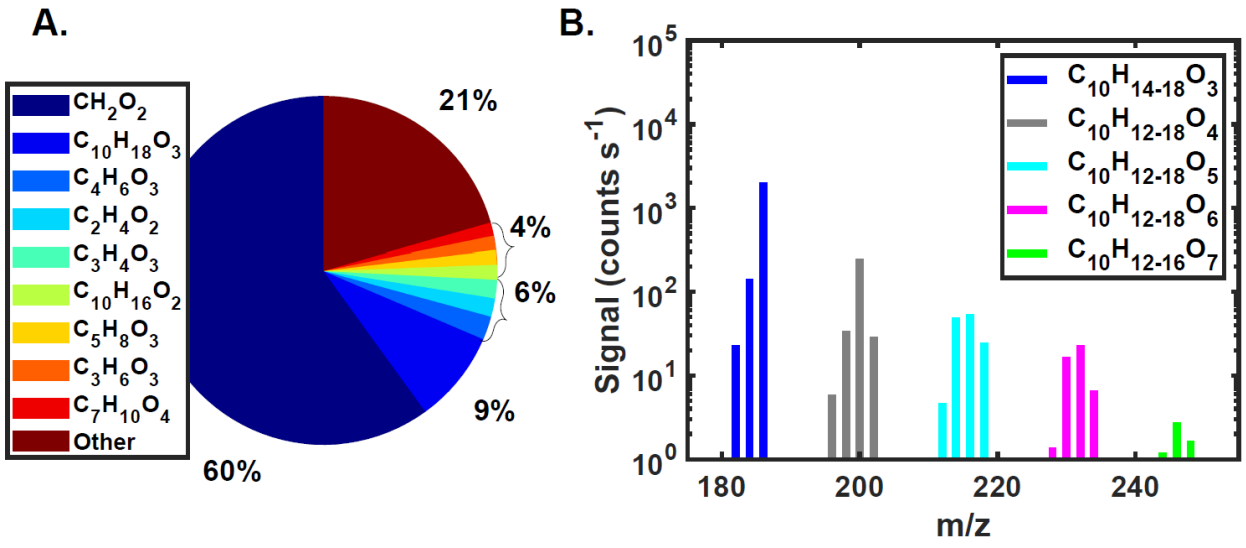

Figure 1. Gas-phase products of Δ3-carene photochemical oxidation. A. Largest CIMS signals, and B. mass spectrum of $C_{10}H_{12\text{-}18}O_{3\text{-}7}$ compounds, separated by 2 hydrogens.

We identified ~200 organic molecular adducts to iodide ions from Δ3-carene photochemical oxidation using the FIGAERO-CIMS. In the gas phase, the dominant signal is formic acid, CH_2O_2 (Fig. 1A), consistent with previous work showing formic acid is a major product[14]. The next largest signal is $C_{10}H_{18}O_3$, presumably a hydroxy hydroperoxide (Scheme 1, *M2*) formed via oxidation of the double bond, which is expected given the use of H_2O_2 as a radical OH precursor which produces abundant HO_2[43]. $C_{10}H_{16}O_2$ is likely caronaldehyde which was previously shown to form in high yields: 31-77% in the presence of NO_x[12, 13, 19], although much lower (14%) in the absence of NO_x[14]. Most of the 10 highest abundance gas-phase species by signal have relatively low oxygen numbers and smaller carbon backbones ($<C_{10}$), however, some higher order oxygenates are detected. Figure 1B shows a series of $C_{10}H_{12\text{-}18}O_{3\text{-}7}$ compounds. Higher oxygen numbers are associated with lower gas-phase concentrations, likely due to a combination of lower yields of highly oxygenated compounds and such species being sequestered into the particle phase and chamber walls due to lower vapor pressures and thus stronger partitioning[44]. We are unaware of other studies reporting Δ3-carene photochemical oxidation products with 10 carbon atoms and more than four oxygen atoms.

Photochemical oxidation of Δ3-carene under the conditions described above produced 4.7 μg m^{-3} of SOA at steady state, corresponding to an SOA mass yield of 31%. The composition of the particle phase (Fig. 2A and B) differs from the gas phase, as expected. The oxygen content is in general significantly higher in the particle phase, dominated by O_5 and O_6 species as opposed to O_2 and O_3 species in the gas phase. The detected particle-phase compositions imply the presence of certain reaction mechanisms. For example, C_7 compounds indicate the efficient loss of a C_3 group, likely through alkoxy scission after cleavage of the cyclopropyl ring, analogous to the Δ3-carene + NO_3 system[45]. It is not obvious how a C_8 species, the largest molecular signal measured in the particle phase, would be formed from gas-phase chemistry followed by gas-to-particle partitioning alone. However, C_8 species also often dominate the particle-phase composition measured with a FIGAERO-CIMS in the α-pinene photochemical oxidation system (Lopez-Hilfiker et al.[46] and Fig. S1). The gas- and particle-phase composition of α-pinene photochemical oxidation measured during this campaign is provided in the SI for comparison.

The FIGAERO-CIMS can also provide insight into the volatility of the SOA. We compare the campaign-average thermogram, i.e. the average of each individual particle-phase desorption in signal versus temperature space, normalized by maximum signal (Fig. 2C), for Δ3-carene relative to the much more studied α-pinene with the same precursor concentrations (10 ppb BVOC, 1 ppm H_2O_2). The temperature of maximum desorption (T_{max}) for the Δ3-carene bulk SOA thermogram is noticeably higher (93 °C) relative to α-pinene (80 °C), indicating that the Δ3-carene SOA is generally of lower volatility[26]. However, the thermogram for Δ3-carene has a smaller relative contribution from the high-temperature tail and the largest measured signals have large carbon backbones (Fig. 2A) indicating the detection of intact molecules formed in the gas-phase during the experiment and desorbing directly from the particle phase. On the other hand, α-pinene has a much larger relative contribution of signal from the high temperature region and the particle-phase signal is dominated by likely thermal decomposition products (Fig. S1A)[47, 48], suggesting decomposition of ELVOC or larger order structures such as dimers or oligomers. The sum thermogram structures do not definitively indicate volatility however, in that the higher SOA concentration in the Δ3-carene system will favor more partitioning of higher volatility material,

which was recently seen for Δ3-carene ozonolysis[49] and could be the reason for the more distinct peak for Δ3-carene.

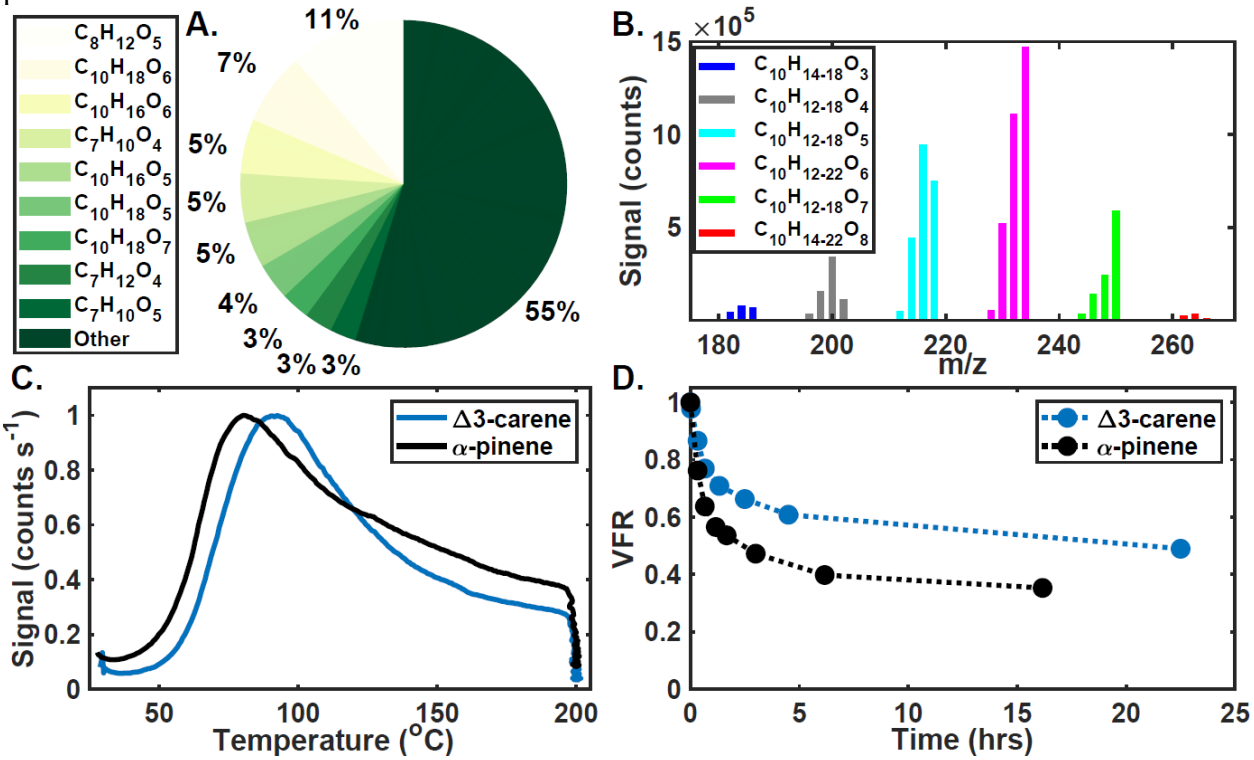

Figure 2. Particle-phase analysis of Δ3-carene photochemical oxidation. A. Top compounds by CIMS signal, B. mass spectrum of $C_{10}H_{12\text{-}22}O_{3\text{-}8}$ compounds, separated by 2 hydrogens, C. Sum thermogram for Δ3-carene (blue) and α-pinene (black), and D. volume fraction remaining (VFR) for 151 nm particles as a function of evaporation time for Δ3-carene (blue) and α-pinene (black).

To provide an additional constraint on effective volatility, we investigate the room-temperature isothermal evaporative behavior of the two SOA systems and find that Δ3-carene SOA is more recalcitrant towards evaporation than is α-pinene SOA formed under similar conditions (Fig. 2C). After 16 hours of isothermal evaporation at room temperature[27], the volume fraction remaining (VFR) for α-pinene SOA is 35%, while after 22.5 hours 49% of the Δ3-carene SOA remains (Fig. 2D). These observations together suggest that Δ3-carene SOA is relatively lower volatility than α-pinene SOA. Given these results, we conclude that Δ3-carene represents a potentially important contribution to ambient SOA. Thus, we explore the initial stages of oxidation to develop an oxidation mechanism and identify potential oxidation products.

3.2 Δ3-carene photochemical oxidation mechanism

A gas-phase mechanism of Δ3-carene photochemical oxidation in the presence of NO_x[50] was developed based on laboratory experiments[16, 17], but to our knowledge no multi-step mechanism exists for photochemical oxidation in the absence of NO_x. Here, we use the measured compositions from the previous section and current understanding of atmospheric chemistry of organic radicals to propose a mechanism for Δ3-carene + OH in a NO_x-free environment via autoxidation (Scheme 1). We start with an OH addition to the double bond resulting in a carbon-centered radical on the tertiary carbon, previously shown to be the major addition channel[51]. While OH could also add to the other side of the double bond or abstract a hydrogen[51], we focus on the

most likely reaction here and at each subsequent stage. After OH addition, O_2 will add at the radical site, resulting in a peroxy radical with four possible stereoisomers, depending on the side of the ring reacting (Scheme 1, *M1*)[34]. We then assume three fates of this peroxy radical: 1) H-shift reactions (isomerization), 2) termination via HO_2, dominant in the chamber experiments described above (Scheme 1, *M2*), or 3) bimolecular reaction with HO_2, RO_2 or NO yielding an alkoxy radical (Scheme 1, *M3*). *M3* could also be formed via photolysis of the closed-shell *M2*. From here, we calculate the rate coefficients of different likely reactions of these first-generation radicals, and further reactions of two second-generation products that are likely to be formed in high yields. Each of these pathways are described in detail below and shown in Scheme 1.

3.2.1 First Generation RO_2 H-shifts

The first generation RO_2 (Scheme 1, *M1*) can undergo two types of bimolecular reactions. The first is termination via HO_2 to a hydroperoxide (Scheme 1, *M2*) which will not condense to aerosol due to the relatively high saturation vapor concentration (1.9×10^3 - 9×10^3 μg m^{-3}, depending on the stereoisomer, as estimated with COSMOtherm[52] and as described in Kurtén et al.[53]). However, being a likely high yield product in our chamber (the second largest composition by signal, Fig. 1A), we perform further calculations on this termination product, discussed in Section 3.2.4. Reaction with HO_2 in our chamber or NO or RO_2 in the atmosphere could also lead to an alkoxy radical (Scheme1, *M3*). Alkoxy radicals are reactive, and we discuss the fate of this molecule in depth in the next section.

We investigate three H-shifts for the peroxy radical (Scheme 1, *M1*): from the α carbon with the -OH group (1,4), from the -OH group on the α carbon (1,5), or from the methyl group on the 3-membered ring (1,7). However, none of these H-shift reactions are likely to be competitive with bimolecular reactions in our laboratory experiments or in any atmospheric conditions, as has been shown previously[34]. The calculated highest rate coefficients of the possible stereoisomers are 5.5×10^{-5} s^{-1} for the 1,4 shift, 1.7×10^{-3} s^{-1} for the 1,5 shift, and 2.6×10^{-6} s^{-1} for the 1,7 shift (Table S1). The corresponding H-shifts were also calculated to be slow ($<10^{-4}$ s^{-1}) in the Δ3-carene + NO_3 system[54].

The product of the H-shift from the α carbon will be a ketone, terminating this pathway and not leading to HOM or otherwise low volatility product. The H-shift from the -OH group produces a hydroperoxy alkoxy radical which has the potential to break open the ring but the formation of this alkoxy is not likely. Neither of these products are investigated further. The fate of the carbon-centered radical on the methyl group attached to the cyclopropyl ring will not be explored further either, as its formation is also unlikely, although the fate of a similar carbon-centered radical is discussed in Section 3.2.3 and can be used as a framework for the fate of this radical.

Scheme 1. Simplified mechanism of Δ3-carene photochemical oxidation. Pathways studied herein are shown in black with compounds labeled "*M#*". Isomerization (H-shift) reactions and cyclopropyl ring-opening reactions that are discussed are highlighted in blue and green, respectively. Carbons are numbered on the parent Δ3-carene for ease of reference in the main text. Speculative autoxidation pathways discussed in section 3.2.5 are shown via gray and colored structures stemming from *M5* and labeled with letters *a-j*.

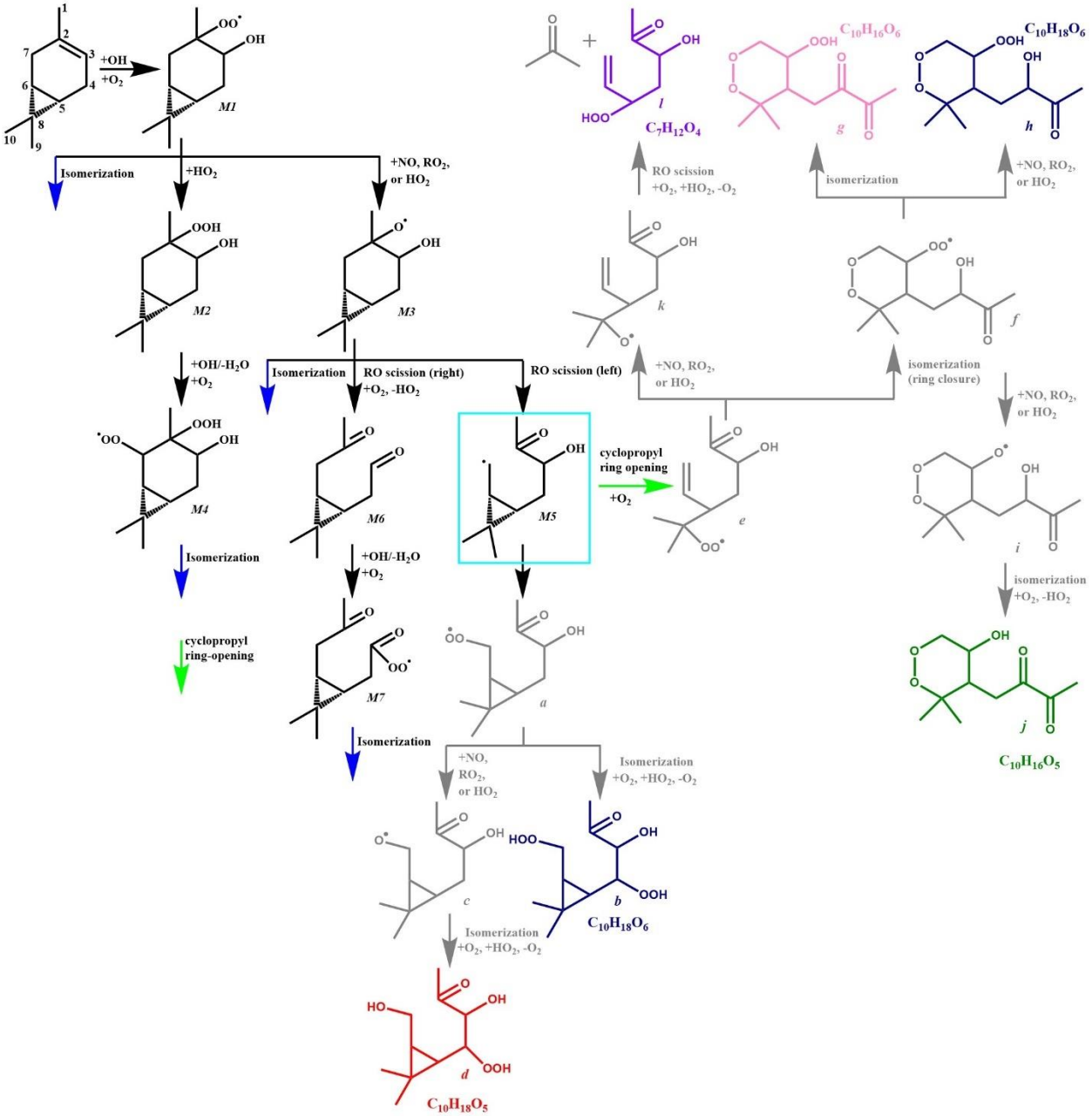

3.2.2 Fate of the First Generation Alkoxy

The hydroxy alkoxy radical (Scheme 1, *M3*), formed from the bimolecular reaction of the first generation RO_2 with HO_2, NO, or RO_2, is an intriguing precursor for HOM and low volatility product formation. The alkoxy alcohol has two likely fates: breaking the six-membered ring,

resulting in *M5* and *M6*, or abstracting a hydrogen from one of the methyl groups on the three-membered ring, which is sterically accessible to the alkoxy radical in the 3D structure (Fig. S2). The cyclohexyl ring can break either towards C7, the CH_2 group labeled "7" on Δ3-carene in Scheme 1, resulting in *M5*, or towards C3, the CH-OH group labeled "3" on Δ3-carene in Scheme 1, resulting in *M6* after abstraction of the alcohol's hydrogen via O_2. The branching will favor breaking towards C3 due to the stabilization from the -OH electron-withdrawing group, leading to caronaldehyde (Scheme 1, *M6*)[55], which we further investigate in Section 3.2.4 due to the potentially high yields. However, we calculate that both reactions have large rate constants (left: $1.1 \times 10^7 - 2.1 \times 10^9$ s^{-1}, right: $1.3 \times 10^9 - 1.2 \times 10^{10}$ s^{-1}) with low barrier heights (left: 4.6 – 8.2 kcal mol^{-1}, right: 4.0-5.5 kcal mol^{-1}) for each stereoisomer (Table 1), indicating the ring break towards C7 can occur in competition with ring break towards C3. If the ring breaks towards C7, this could lead to HOM either by O_2 addition and further H-shift reactions (see Section 3.2.5 and Scheme 1) or lead to the breaking of the cyclopropyl ring (see next section) which has been shown to be important for HOM formation in the Δ3-carene + NO_3 system[45, 54]. Even low yields of HOM can impact SOA formation due to their often very low volatility, implying small fractions breaking towards C7 are still atmospherically relevant. Because the ring breaking towards C7 and C3 are close in rates and barrier heights, F12 single point corrections are included in the alkoxy ring breaking rate coefficient calculations to increase precision.

The alkoxy radical can also perform H-shifts. We investigated three different H-shifts (Table 1) and found that only the shift from one of the methyl groups on the propyl ring could be competitive with ring breaking. This shift will be approximately as likely as the ring breaking towards C7, with rate coefficients of 5.8×10^7 and 6.6×10^7 s^{-1} for the two stereoisomers where this shift is geometrically available. It is generally assumed that H-abstractions from primary carbons are slow[56], although recent findings suggest for specific systems, they may be competitive[57]. We therefore include F12 single point energy calculations in these H-shifts as well, to compare with the alkoxy ring breaking as accurately as possible. We explore the fate of the resulting primary carbon-centered radical in the next section. The other possible H-shifts are predicted to be much slower than the methyl H-shifts and the ring breaking reactions, so these do not include F12 single-point calculations. Table 1 details the rate constants and barrier heights for each of these reactions.

Table 1. Fate of the first-generation alkoxy radical, *M3* from Scheme 1. Rate coefficients (units of s^{-1}) and forward barriers (units of kcal mol^{-1}) are shown for each stereoisomer. Blue values indicate the inclusion of F12 single point corrections, black values are calculated with barrier heights at the ωB97X-D/aug-cc-pVTZ level.

	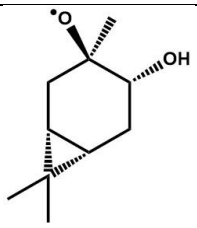	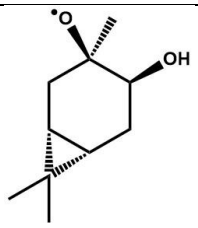	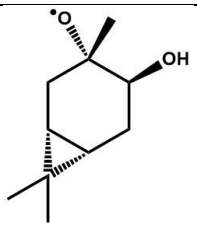	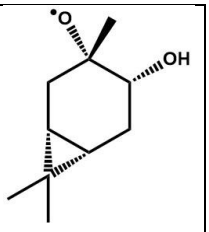
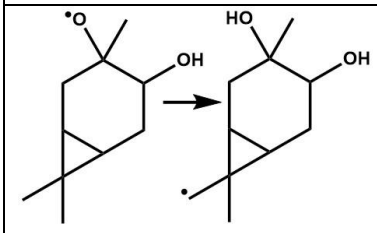	not possible for this isomer*	not possible for this isomer*	5.8×10^{7} s^{-1} 7.0 kcal mol^{-1}	6.6×10^{7} s^{-1} 7.1 kcal mol^{-1}
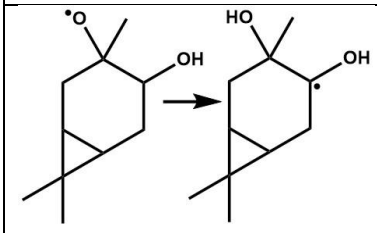	10 s^{-1} 19.3 kcal mol^{-1}	not possible for this isomer*	1.7×10^{-2} s^{-1} 23.6 kcal mol^{-1}	not possible for this isomer*
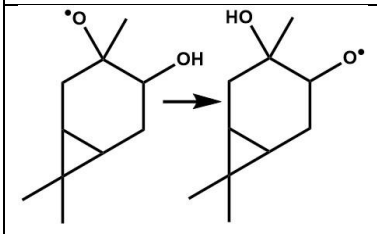	not possible for this isomer*	Ring breaks open during ωB97X-D optimization	not possible for this isomer*	Ring breaks open during ωB97X-D optimization
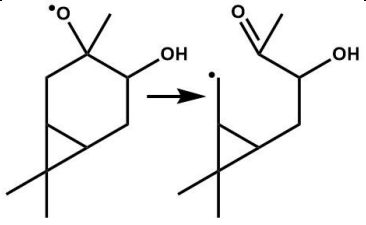	6.1×10^{7} s^{-1} 7.6 kcal mol^{-1}	2.1×10^{9} s^{-1} 4.6 kcal mol^{-1}	1.1×10^{7} s^{-1} 8.2 kcal mol^{-1}	7.1×10^{7} s^{-1} 7.1 kcal mol^{-1}
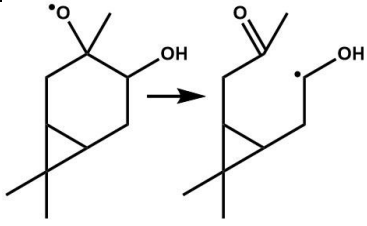	1.1×10^{10} s^{-1} 4.2 kcal mol^{-1}	5.6×10^{9} s^{-1} 4.4 kcal mol^{-1}	1.2×10^{10} s^{-1} 4.0 kcal mol^{-1}	1.3×10^{9} s^{-1} 5.5 kcal mol^{-1}

*steric hindrance prevents this reaction from occurring in the isomer in question

3.2.3 Cyclopropyl ring opening

As described above, opening of the cyclopropyl ring could be an important pathway to HOM formation[45, 54], so we studied this reaction in greater depth (Table S2). The primary carbon-centered radical α to the cyclopropyl ring, be it formed via H-abstraction from the methyl group (Table S2, reactant in the first two rows) or from the breaking of the cyclohexyl ring (Table S2, reactant in the bottom row), has two main fates. The first is addition of an O_2 to form a peroxy radical, assumed to occur at ~10^7 - 10^8 s^{-1} under atmospheric conditions[11, 58, 59]. In competition with this bimolecular reaction, the radical may also be able to break open the cyclopropyl ring, forming a double bond and a more stable secondary or tertiary carbon-centered radical. We calculated the rate constants for the cyclopropyl ring openings and found them to be fast, on the order of 10^7-10^8 s^{-1} (Table S2). Thus, we anticipate contributions from both O_2 addition and ring opening. We expect these products to be good candidates to form HOM, as breaking the cyclopropyl ring will increase the flexibility and therefore the ability to perform further H-shifts after O_2 addition, particularly in the case where the cyclohexyl ring is also already broken (Table S2, bottom row). Furthermore, the double bond that is generated in each of the three cases will be reactive to OH addition, leading to further oxidation with the potential for additional H-shifts or peroxy ring closing reactions and a lowering of the volatility[34].

3.2.4 Fate of Second-Generation Products

HOM formation from second-generation products will not be prompt, due to the inherent time required to form the reactant, i.e. the first-generation product, but their isomerization rates will typically be enhanced due to the presence of multiple functional groups[5, 32] and multi-generation SOA formation is well documented[60-66]. As stated above, caronaldehyde (Scheme 1, *M6*) is a first-generation product with widely varying observed yields (14-77%)[12-15], and measured to be 1% of total gas-phase signal here (Fig. 1A), although signal does not equate to overall concentration and iodide CIMS is not expected to be especially sensitive to caronaldehyde[25]. Due to its potentially high yields we investigate its fate further. The most likely reaction pathway for caronaldehyde is the abstraction of the aldehyde hydrogen via OH[61, 67, 68], followed by O_2 addition, yielding a second generation RO_2 (Scheme 1, *M7*). This RO_2 can then undergo reaction with HO_2 to form a carboxylic acid[69-71] or a peroxy acid, both of which are estimated to have relatively high vapor pressures (carboxylic acid: 1.2×10^3 μg m^{-3}, peroxy acid: 50 μg m^{-3} [52]), or the RO_2 can undergo an H-shift. We investigated a 1,7 H-shift from the carbon α to the ketone and found that it is not likely to compete with bimolecular reaction, as the calculated rate constant is 2.4-2.9 $\times 10^{-4}$ s^{-1} (Table S3). We conclude that this pathway likely does not lead to HOM formation.

The other second-generation product we investigate is the hydroxy hydroperoxide (Scheme 1 *M2*, and Table S4) which is the second largest gas-phase signal measured (9%, Fig. 1A) in our chamber. One option for further oxidation of this molecule is an H-abstraction from the molecule via OH. The most likely H-abstraction is from C3[61, 67, 68] or the -OH group on C3, although this will likely terminate in a ketone. To investigate a possible second-generation H-shift, we assume an H-abstraction from C7 (Scheme 1), followed by O_2 addition to form *M4*, and an H-shift from C3, leading to the formation of a ketone. We calculate the rate coefficient of the H-shift for each of the four possible peroxy stereoisomers and find them to be slow (0.6-36 $\times 10^{-9}$ s^{-1}) and therefore unlikely (Table S4). This is meant to be a representative test of peroxy radical H-shifts stemming from *M2*. Peroxy radicals located at different positions on the molecule may have faster H-shifts, although it is likely that they will still abstract the hydrogen from C3 as it is the most acidic[61, 67, 68], terminating the molecule as a ketone that will be of relatively high volatility (9-110 μg m^{-3},

depending on the stereoisomer[52]). The second generation peroxy radical (Scheme 1, *M4*) could also abstract the hydrogen off the -OOH or the -OH group, which could lead to further unimolecular reactions and potential oxygenation, although we do not explore these possibilities here.

3.2.5 Potential Reactions

Figures 1A and 2A show the molecular compositions of species measured in the gas and particle phase, respectively. The only overlap with our computationally developed mechanism (Scheme 1) is $C_{10}H_{18}O_3$, presumably a hydroxy hydroperoxide, and $C_{10}H_{16}O_2$, presumably caronaldehyde. Additionally, in Section 3.2.2, we speculated based on previous work[45, 54] that breaking the cyclohexyl ring towards C7 via an alkoxy (Scheme 1, *M3*) is a likely path toward HOM formation. To fill the gap between measured and modeled species, we present possible reactions leading to several of the measured compositions in the particle phase (Scheme 1, gray and colored compounds), some of which are HOM (i.e. containing six or more oxygens), from the carbon-centered radical intermediate (Scheme 1, *M5*). Throughout this discussion, we do not address all possible reaction pathways and products, simply the most likely or those that lead to measured compositions via autoxidation. We note that biomolecular reactions likely produce many of the same molecular compositions discussed in this section, although we do not explore them herein. We also do not show every possible H-shift location for a molecule but choose one for illustration. Many of these reactions are analogous to those probed in Scheme 1 of Draper et al.[45], where NO_3 was the oxidant rather than OH, leading to slightly different functionalization.

There are two direct fates of the carbon-centered radical (Scheme 1, *M5*). First, O_2 could add to the carbon-centered radical, forming a peroxy radical (*a*), which can then terminate as $C_{10}H_{18}O_6$ (*b*, navy), or $C_{10}H_{18}O_5$ (*d*, red). Second, the carbon-centered radical (Scheme 1, *M5*) could rearrange, opening the cyclopropyl ring as discussed in section 3.2.3 and Table S2, followed by O_2 addition, leading to a peroxy radical (*e*). The peroxy radical (*e*) could perform a ring closure + O_2 addition (*f*) and then either terminate to another isomer of $C_{10}H_{18}O_6$ (*h*, navy), perform an H-shift to form $C_{10}H_{16}O_6$ (*g*, pink), or become an alkoxy which then performs an H-shift to generate $C_{10}H_{16}O_5$ (*j*, green). Finally, the peroxy radical (*e*) could become an alkoxy (*k*), which could lose acetone to form $C_7H_{12}O_4$ (*l*, purple). In all, we predict five molecular compositions from this one radical intermediate (Scheme 1, *M5*).

A few overarching themes, along with some further questions, arise from the speculative mechanism. First, we find multiple possible isomers of $C_{10}H_{18}O_6$ (Scheme 1, *b* and *h*), a reminder that each molecular formula measured likely contains multiple isomers, possibly with varying I^- CIMS sensitivity. Second, we find that the O_5 species (*d* and *j*) are generated from alkoxy radicals (*c* and *i*), while we predict that the C_7 (*l*), of which there are three in the top 10 measured particle-phase signals (Fig. 2A), is the result of cleavage of the cyclopropyl ring followed by alkoxy scission to remove three carbons. Both the O_5 and O_7 pathways we propose are expected to be enhanced with increasing NO_x concentrations because they both stem from alkoxy radicals.

We note that our mechanistic speculations are based on the assumption that products measured in the particle phase are produced in the gas phase, which may not necessarily be true. For example, $C_7H_{12}O_4$ is the eighth most abundant signal in the particle phase (Fig. 2A) yet is expected to have a relatively high volatility: the structure predicted in Scheme 1 is predicted to have a saturation vapor concentration of 340 - 470 μg m^{-3}, depending on the stereoisomer[52]. Instead of forming in the gas phase and then condensing, the $C_7H_{12}O_4$ could instead be formed via thermal decomposition of a different particle-phase species during thermal desorption, as shown

previously[47, 48, 72]. However, for $C_7H_{12}O_4$, the thermogram does not show typical signs of thermal decomposition (Fig. S3).

Similar to α-pinene, some Δ3-carene products retain the same degree of unsaturation (DOU) as the parent compound while simultaneously becoming more oxygenated and lower volatility. Δ3-Carene has three DOU (two rings and one double bond), as do for example $C_{10}H_{16}O_n$ and $C_7H_{10}O_n$ species, and $C_8H_{12}O_5$, the largest signal measured in the particle phase (Fig. 2A). This pattern is most likely to occur via carbonyl functionalities and in some cases the formation of endoperoxides which are important in other BVOC oxidation systems[8, 73]. Two structural examples are the dihydroperoxy ketone that is likely to form from the second-generation H-shift of the hydroxy hydroperoxide discussed in section 3.2.4, or molecules *g* and *j* in Scheme 1. However, the addition of endoperoxides or ketones is not expected to lower the volatility substantially: the predicted vapor concentration of molecule *g* in Scheme 1 is 80-140 μg m^{-3}, while the ketone formed from the H-shift in Table S4 and discussed in the previous section is 9-110 μg m^{-3}, depending on the stereoisomer[52]. If instead the carbonyls were part of carboxylic or peroxy acid groups, the vapor pressure would likely be much lower[74].

4 Atmospheric Implications

We found that the first generation RO_2 (Scheme 1, *M1*) is most likely to form an alkoxy radical (Scheme 1, *M3*) in competition with terminating channels of bimolecular reaction. Those alkoxy radicals will predominantly break the cyclohexyl ring towards C3, the carbon to which OH initially adds, and form caronaldehyde (Scheme 1, *M6*). However, we calculate that a non-negligible fraction will ring-break towards C7, a CH_2 group (Scheme 1, *M5*), from which it is easier to develop plausible mechanisms for HOM formation (Scheme S1). Additionally, some of these alkoxy radicals are likely to undergo H-shifts from the methyl group on the cyclopropyl ring, which could lead to opening the cyclopropyl ring, and likely to HOM, as well as to seven-carbon products detected in the chamber study. If the first generation RO_2 terminates in a hydroxy hydroperoxide (Scheme 1, *M2*), it can undergo H-abstraction via OH, although the resulting molecule will not likely undergo H-shifts and is instead expected to terminate in a dihydroperoxy ketone. The RO_2 resulting from the OH oxidation via H-abstraction from caronaldehyde (Scheme 1, *M7*) is also unlikely to undergo H-shifts. Therefore, both second generation RO_2 are most likely to terminate with HO_2 to form ROOHs. The RO_2 could however also form RO, which are more likely to lead to HOM, although RO formation is less likely in the case of caronaldehyde where the RO would be an acyl RO that is likely to decompose and lose CO_2. In light of these considerations, we conclude that the main pathway for forming HOM from OH oxidation of Δ3-carene will likely be from alkoxy ring breaking towards C7 (Scheme 1, *M5*).

An interesting finding of this work is the surprisingly rapid abstraction of primary H's from methyl groups by alkoxy radicals, which is generally assumed to be slow[56], but has been calculated to be rapid in the α-pinene system[57]. More work is needed to investigate the possibility of these types of isomerization reactions in other BVOC, particularly monoterpenes that tend to have multiple methyl groups. Additionally, mechanisms describing how a molecule can retain the DOU of the parent compound while being oxidized to products of sufficiently low volatility to partition to the particle phase, for example $C_{10}H_{16}O_6$, are still unclear. HOM with multiple DOU have been observed in the gas phase[8, 75], but the predicted structures are typically multifunctional bicyclic or contain carboxylic acids[75], which we do not predict in Scheme 1.

Supporting Information

Figures depicting α-pinene oxidation products, volatility of a Δ3-carene photochemical oxidation product, and a 3D compound. Tables with rate coefficients and barrier heights for reactions studied.

Acknowledgements

This research was supported by funding from the Academy of Finland, the Independent Research Fund Denmark (9040-00142B), the High Performance Computing Center at the University of Copenhagen, and a grant to JAT from the U.S. National Science Foundation (CHE-1807204). Chamber measurements were supported in part by a grant from the U.S. Department of Energy DE-SC0018221. ELD was supported by the National Science Foundation Graduate Research Fellowship under grant no. DGE-1256082 and GROW travel grant. PNNL authors were supported by the U.S. Department of Energy, Office of Biological and Environmental Research, as part of the ASR program. Pacific Northwest National Laboratory is operated for DOE by Battelle Memorial Institute under contract DE-AC05-76RL01830. We thank the CSC-IT Center for Science in Espoo, Finland, for computational resources. We thank Havala Pye, Ivan Piletic, Donna Schwede, and Kiran Alapaty of the EPA for reviewing the manuscript. The views expressed in this article are those of the authors and do not necessarily represent the views or policies of the U.S. Environmental Protection Agency. It has been subjected to Agency administrative review and approved for publication.

Present Addresses

[!]Present address: Office of Research and Development, US Environmental Protection Agency, Research Triangle Park, NC, 27711, USA

[@]Present address: Department of Chemistry, Nanoscience Center, University of Jyväskylä, Jyväskylä, FI-40014, Finland

[#]Present address: Aerosol Physics Laboratory, Tampere University, Tampere, FI-33014, Finland

[$]Present address: Laboratory of Atmospheric Chemistry, Paul Scherrer Institute, Villigen, CH-5232, Switzerland

[%]Present address: School of Environment, Harbin Institute of Technology, Harbin, Heilongjiang, 150001, China

[^]Present address: Tofwerk AG, Thun, CH-3645, Switzerland

[&]Present address: Department of Applied Physics, University of Eastern Finland, Kuopio, FI-70210, Finland

References

1. Jimenez, J. L.; Canagaratna, M. R.; Donahue, N. M.; Prevot, A. S. H.; Zhang, Q.; Kroll, J. H.; DeCarlo, P. F.; Allan, J. D.; Coe, H.; Ng, N. L.; Aiken, A. C.; Docherty, K. S.; Ulbrich, I. M.; Grieshop, A. P.; Robinson, A. L.; Duplissy, J.; Smith, J. D.; Wilson, K. R.; Lanz, V. A.; Hueglin, C.; Sun, Y. L.; Tian, J.; Laaksonen, A.; Raatikainen, T.; Rautiainen, J.; Vaattovaara, P.; Ehn, M.; Kulmala, M.; Tomlinson, J. M.; Collins, D. R.; Cubison, M. J.; Dunlea, J.; Huffman, J. A.; Onasch, T. B.; Alfarra, M. R.; Williams, P. I.; Bower, K.; Kondo, Y.; Schneider, J.; Drewnick, F.; Borrmann, S.; Weimer, S.; Demerjian, K.; Salcedo, D.; Cottrell, L.; Griffin, R.; Takami, A.; Miyoshi, T.; Hatakeyama, S.; Shimono, A.; Sun, J. Y.; Zhang, Y. M.; Dzepina, K.; Kimmel, J. R.; Sueper, D.; Jayne, J. T.; Herndon, S. C.; Trimborn, A. M.; Williams, L. R.; Wood, E. C.; Middlebrook, A. M.; Kolb, C. E.; Baltensperger, U.; Worsnop, D. R., Evolution of Organic Aerosols in the Atmosphere. *Science* **2009,** *326* (5959), 1525.
2. Zhang, Q.; Jimenez, J. L.; Canagaratna, M. R.; Allan, J. D.; Coe, H.; Ulbrich, I.; Alfarra, M. R.; Takami, A.; Middlebrook, A. M.; Sun, Y. L.; Dzepina, K.; Dunlea, E.; Docherty, K.; DeCarlo, P. F.; Salcedo, D.; Onasch, T.; Jayne, J. T.; Miyoshi, T.; Shimono, A.; Hatakeyama, S.; Takegawa, N.; Kondo, Y.; Schneider, J.; Drewnick, F.; Borrmann, S.; Weimer, S.; Demerjian, K.; Williams, P.; Bower, K.; Bahreini, R.; Cottrell, L.; Griffin, R. J.; Rautiainen, J.; Sun, J. Y.; Zhang, Y. M.; Worsnop, D. R., Ubiquity and dominance of oxygenated species in organic aerosols in anthropogenically-influenced Northern Hemisphere midlatitudes. *Geophysical Research Letters* **2007,** *34* (13), L13801.
3. V. Masson-Delmotte, P. Z., A. Pirani, S.L. Connors, C. Péan, S. Berger, N. Caud, Y. Chen, L. Goldfarb, M. I. Gomis, M. Huang, K. Leitzell, E. Lonnoy, J. B.; R. Matthews, T. K. M., T. Waterfield, O. Yelekçi, R. Yu, B. Zhou *IPCC, 2021: Climate Change 2021: The Physical Science Basis. Contribution of Working Group I to the Sixth Assessment Report of the Intergovernmental Panel on Climate Change*; 2021.
4. Hallquist, M.; Wenger, J. C.; Baltensperger, U.; Rudich, Y.; Simpson, D.; Claeys, M.; Dommen, J.; Donahue, N. M.; George, C.; Goldstein, A. H.; Hamilton, J. F.; Herrmann, H.; Hoffmann, T.; Iinuma, Y.; Jang, M.; Jenkin, M. E.; Jimenez, J. L.; Kiendler-Scharr, A.; Maenhaut, W.; McFiggans, G.; Mentel, T. F.; Monod, A.; Prevot, A. S. H.; Seinfeld, J. H.; Surratt, J. D.; Szmigielski, R.; Wildt, J., The formation, properties and impact of secondary organic aerosol: current and emerging issues. *Atmos. Chem. Phys.* **2009,** *9* (14), 5155-5236.
5. Crounse, J. D.; Nielsen, L. B.; Jørgensen, S.; Kjaergaard, H. G.; Wennberg, P. O., Autoxidation of Organic Compounds in the Atmosphere. *The Journal of Physical Chemistry Letters* **2013,** *4* (20), 3513-3520.
6. Bianchi, F.; Kurtén, T.; Riva, M.; Mohr, C.; Rissanen, M. P.; Roldin, P.; Berndt, T.; Crounse, J. D.; Wennberg, P. O.; Mentel, T. F.; Wildt, J.; Junninen, H.; Jokinen, T.; Kulmala, M.; Worsnop, D. R.; Thornton, J. A.; Donahue, N.; Kjaergaard, H. G.; Ehn, M., Highly Oxygenated Organic Molecules (HOM) from Gas-Phase Autoxidation Involving Peroxy Radicals: A Key Contributor to Atmospheric Aerosol. *Chemical Reviews* **2019,** *119* (6), 3472-3509.
7. Sindelarova, K.; Granier, C.; Bouarar, I.; Guenther, A.; Tilmes, S.; Stavrakou, T.; Müller, J. F.; Kuhn, U.; Stefani, P.; Knorr, W., Global data set of biogenic VOC emissions calculated by the MEGAN model over the last 30 years. *Atmos. Chem. Phys.* **2014,** *14* (17), 9317-9341.
8. Iyer, S.; Rissanen, M. P.; Valiev, R.; Barua, S.; Krechmer, J. E.; Thornton, J.; Ehn, M.; Kurtén, T., Molecular mechanism for rapid autoxidation in α-pinene ozonolysis. *Nature Communications* **2021,** *12* (1), 878.
9. Fry, J. L.; Draper, D. C.; Zarzana, K. J.; Campuzano-Jost, P.; Day, D. A.; Jimenez, J. L.; Brown, S. S.; Cohen, R. C.; Kaser, L.; Hansel, A.; Cappellin, L.; Karl, T.; Hodzic Roux, A.; Turnipseed, A.; Cantrell, C.; Lefer, B. L.; Grossberg, N., Observations of gas- and aerosol-phase organic nitrates at BEACHON-RoMBAS 2011. *Atmos. Chem. Phys.* **2013,** *13* (17), 8585-8605.

10. Hantschke, L.; Novelli, A.; Bohn, B.; Cho, C.; Reimer, D.; Rohrer, F.; Tillmann, R.; Glowania, M.; Hofzumahaus, A.; Kiendler-Scharr, A.; Wahner, A.; Fuchs, H., Atmospheric photooxidation and ozonolysis of Δ3-carene and 3-caronaldehyde: rate constants and product yields. *Atmos. Chem. Phys.* **2021,** *21* (16), 12665-12685.
11. Atkinson, R., Gas-Phase Tropospheric Chemistry of Volatile Organic Compounds: 1. Alkanes and Alkenes. *Journal of Physical and Chemical Reference Data* **1997,** *26* (2), 215-290.
12. Arey, J.; Atkinson, R.; Aschmann, S. M., Product study of the gas-phase reactions of monoterpenes with the OH radical in the presence of NO x. *Journal of Geophysical Research: Atmospheres* **1990,** *95* (D11), 18539-18546.
13. Hakola, H.; Arey, J.; Aschmann, S. M.; Atkinson, R., Product formation from the gas-phase reactions of OH radicals and O3 with a series of monoterpenes. *Journal of Atmospheric Chemistry* **1994,** *18* (1), 75-102.
14. Larsen, B. R.; Di Bella, D.; Glasius, M.; Winterhalter, R.; Jensen, N. R.; Hjorth, J., Gas-Phase OH Oxidation of Monoterpenes: Gaseous and Particulate Products. *Journal of Atmospheric Chemistry* **2001,** *38* (3), 231-276.
15. Van den Bergh, V.; Coeckelberghs, H.; Vankerckhoven, H.; Compernolle, F.; Vinckier, C., Study of the carbonyl products of terpene/OH radical reactions: detection of the 2,4-DNPH derivatives by HPLC-MS. *Analytical and Bioanalytical Chemistry* **2004,** *379* (3), 484-494.
16. Hoffmann, T.; Odum, J. R.; Bowman, F.; Collins, D.; Klockow, D.; Flagan, R. C.; Seinfeld, J. H., Formation of Organic Aerosols from the Oxidation of Biogenic Hydrocarbons. *Journal of Atmospheric Chemistry* **1997,** *26* (2), 189-222.
17. Griffin, R. J.; Cocker Iii, D. R.; Flagan, R. C.; Seinfeld, J. H., Organic aerosol formation from the oxidation of biogenic hydrocarbons. *Journal of Geophysical Research: Atmospheres* **1999,** *104* (D3), 3555-3567.
18. Varutbangkul, V.; Brechtel, F. J.; Bahreini, R.; Ng, N. L.; Keywood, M. D.; Kroll, J. H.; Flagan, R. C.; Seinfeld, J. H.; Lee, A.; Goldstein, A. H., Hygroscopicity of secondary organic aerosols formed by oxidation of cycloalkenes, monoterpenes, sesquiterpenes, and related compounds. *Atmos. Chem. Phys.* **2006,** *6* (9), 2367-2388.
19. Lee, A.; Goldstein, A. H.; Kroll, J. H.; Ng, N. L.; Varutbangkul, V.; Flagan, R. C.; Seinfeld, J. H., Gas-phase products and secondary aerosol yields from the photooxidation of 16 different terpenes. *Journal of Geophysical Research: Atmospheres* **2006,** *111* (D17), D17305.
20. Pye, H. O. T.; D'Ambro, E. L.; Lee, B. H.; Schobesberger, S.; Takeuchi, M.; Zhao, Y.; Lopez-Hilfiker, F.; Liu, J.; Shilling, J. E.; Xing, J.; Mathur, R.; Middlebrook, A. M.; Liao, J.; Welti, A.; Graus, M.; Warneke, C.; de Gouw, J. A.; Holloway, J. S.; Ryerson, T. B.; Pollack, I. B.; Thornton, J. A., Anthropogenic enhancements to production of highly oxygenated molecules from autoxidation. *Proceedings of the National Academy of Sciences* **2019,** *116* (14), 6641.
21. Fang, W.; Gong, L.; Sheng, L., Online analysis of secondary organic aerosols from OH-initiated photooxidation and ozonolysis of α-pinene, β-pinene, Δ^3-carene and d-limonene by thermal desorption–photoionisation aerosol mass spectrometry. *Environmental Chemistry* **2017,** *14* (2), 75-90.
22. Liu, S.; Shilling, J. E.; Song, C.; Hiranuma, N.; Zaveri, R. A.; Russell, L. M., Hydrolysis of organonitrate functional groups in aerosol particles. *Aerosol Sci. Technol.* **2012,** *46* (12), 1359-1369.
23. D'Ambro, E. L.; Schobesberger, S.; Gaston, C. J.; Lopez-Hilfiker, F. D.; Lee, B. H.; Liu, J. M.; Zelenyuk, A.; Bell, D.; Cappa, C. D.; Helgestad, T.; Li, Z. Y.; Guenther, A.; Wang, J.; Wise, M.; Caylor, R.; Surratt, J. D.; Riedel, T.; Hyttinen, N.; Salo, V. T.; Hasan, G.; Kurten, T.; Shilling, J. E.; Thornton, J. A., Chamber-based insights into the factors controlling epoxydiol (IEPOX) secondary organic aerosol (SOA) yield, composition, and volatility. *Atmos. Chem. Phys.* **2019,** *19* (17), 11253-11265.

24. Li, Z.; D'Ambro, E. L.; Schobesberger, S.; Gaston, C. J.; Lopez-Hilfiker, F. D.; Liu, J.; Shilling, J. E.; Thornton, J. A.; Cappa, C. D., A robust clustering algorithm for analysis of composition-dependent organic aerosol thermal desorption measurements. *Atmos. Chem. Phys.* **2020,** *20* (4), 2489-2512.
25. Lee, B. H.; Lopez-Hilfiker, F. D.; Mohr, C.; Kurten, T.; Worsnop, D. R.; Thornton, J. A., An iodide-adduct high-resolution time-of-flight chemical-ionization mass spectrometer: application to atmospheric inorganic and organic compounds. *Environ. Sci. Technol.* **2014,** *48* (11), 6309-17.
26. Lopez-Hilfiker, F. D.; Mohr, C.; Ehn, M.; Rubach, F.; Kleist, E.; Wildt, J.; Mentel, T. F.; Lutz, A.; Hallquist, M.; Worsnop, D.; Thornton, J. A., A novel method for online analysis of gas and particle composition: description and evaluation of a Filter Inlet for Gases and AEROsols (FIGAERO). *Atmos. Meas. Tech.* **2014,** *7* (4), 983-1001.
27. Vaden, T. D.; Imre, D.; Beranek, J.; Shrivastava, M.; Zelenyuk, A., Evaporation kinetics and phase of laboratory and ambient secondary organic aerosol. *Proc. Natl. Acad. Sci. U. S. A.* **2011,** *108* (6), 2190-2195.
28. Møller, K. H.; Otkjær, R. V.; Hyttinen, N.; Kurtén, T.; Kjaergaard, H. G., Cost-Effective Implementation of Multiconformer Transition State Theory for Peroxy Radical Hydrogen Shift Reactions. *J. Phys. Chem. A* **2016,** *120* (51), 10072-10087.
29. Vereecken, L.; Peeters, J., The 1,5-H-shift in 1-butoxy: A case study in the rigorous implementation of transition state theory for a multirotamer system. *The Journal of Chemical Physics* **2003,** *119* (10), 5159-5170.
30. Praske, E.; Otkjær, R. V.; Crounse, J. D.; Hethcox, J. C.; Stoltz, B. M.; Kjaergaard, H. G.; Wennberg, P. O., Atmospheric autoxidation is increasingly important in urban and suburban North America. *Proceedings of the National Academy of Sciences* **2018,** *115* (1), 64.
31. Chen, J.; Møller, K. H.; Wennberg, P. O.; Kjaergaard, H. G., Unimolecular Reactions Following Indoor and Outdoor Limonene Ozonolysis. *J. Phys. Chem. A* **2021,** *125* (2), 669-680.
32. Otkjær, R. V.; Jakobsen, H. H.; Tram, C. M.; Kjaergaard, H. G., Calculated Hydrogen Shift Rate Constants in Substituted Alkyl Peroxy Radicals. *J. Phys. Chem. A* **2018,** *122* (43), 8665-8673.
33. Møller, K. H.; Berndt, T.; Kjaergaard, H. G., Atmospheric Autoxidation of Amines. *Environmental Science & Technology* **2020,** *54* (18), 11087-11099.
34. Møller, K. H.; Otkjær, R. V.; Chen, J.; Kjaergaard, H. G., Double Bonds Are Key to Fast Unimolecular Reactivity in First-Generation Monoterpene Hydroxy Peroxy Radicals. *J. Phys. Chem. A* **2020,** *124* (14), 2885-2896.
35. Wavefunction, I. *Spartan '16*, Irvine, CA.
36. Frisch, M. J.; Trucks, G. W.; Schlegel, H. B.; Scuseria, G. E.; Robb, M. A.; Cheeseman, J. R.; Scalmani, G.; Barone, V.; Mennucci, B.; Petersson, G. A.; Nakatsuji, H.; Caricato, M.; Li, X.; Hratchian, H. P.; Izmaylov, A. F.; Bloino, J.; Zheng, G.; Sonnenberg, J. L.; Hada, M.; Ehara, M.; Toyota, K.; Fukuda, R.; Hasegawa, J.; Ishida, M.; Nakajima, T.; Honda, Y.; Kitao, O.; Nakai, H.; Vreven, T.; Montgomery-Jr., J. A.; Peralta, J. E.; Ogliaro, F.; Bearpark, M.; Heyd, J. J.; Brothers, E.; Kudin, K. N.; Staroverov, V. N.; Keith, T.; Kobayashi, R.; Normand, J.; Raghavachari, K.; Rendell, A.; Burant, J. C.; Iyengar, S. S.; Tomasi, J.; Cossi, M.; Rega, N.; Millam, J. M.; Klene, M.; Knox, J. E.; Cross, J. B.; Bakken, V.; Adamo, C.; Jaramillo, J.; Gomperts, R.; Stratmann, R. E.; Yazyev, O.; Austin, A. J.; Cammi, R.; Pomelli, C.; Ochterski, J. W.; Martin, R. L.; Morokuma, K.; Zakrzewski, V. G.; Voth, G. A.; Salvador, P.; Dannenberg, J. J.; Dapprich, S.; Daniels, A. D.; Farkas, O.; Foresman, J. B.; Ortiz, J. V.; Cioslowski, J.; Fox, D. J. *Gaussian 09 Rev. D.01*, Wallingford, CT, 2013.
37. Frisch, M. J.; Trucks, G. W.; Schlegel, H. B.; Scuseria, G. E.; Robb, M. A.; Cheeseman, J. R.; Scalmani, G.; Barone, V.; Petersson, G. A.; Nakatsuji, H.; Li, X.; Caricato, M.; Marenich, A. V.; Bloino, J.; Janesko, B. G.; Gomperts, R.; Mennucci, B.; Hratchian, H. P.; Ortiz, J. V.; Izmaylov, A. F.; Sonnenberg, J. L.; Williams-Young, D.; Ding, F.; Lipparini, F.; Egidi, F.; Goings, J.; Peng, B.; Petrone, A.; Henderson, T.; Ranasinghe, D.; Zakrzewski, V. G.; Gao, J.; Rega, N.; Zheng, G.; Liang, W.; Hada, M.;

Ehara, M.; Toyota, K.; Fukuda, R.; Hasegawa, J.; Ishida, M.; Nakajima, T.; Honda, Y.; Kitao, O.; Nakai, H.; Vreven, T.; Throssell, K.; Montgomery Jr., J. A.; Peralta, J. E.; Ogliaro, F.; Bearpark, M. J.; Heyd, J. J.; Brothers, E. N.; Kudin, K. N.; Staroverov, V. N.; Keith, T. A.; Kobayashi, R.; Normand, J.; Raghavachari, K.; Rendell, A. P.; Burant, J. C.; Iyengar, S. S.; Tomasi, J.; Cossi, M.; Millam, J. M.; Klene, M.; Adamo, C.; Cammi, R.; Ochterski, J. W.; Martin, R. L.; Morokuma, K.; Farkas, O.; Foresman, J. B.; Fox, D. J. *Gaussian 16 Rev. B.01*, Wallingford, CT, 2016.

38. Otkjær, R. V. M., K. H. *Removal of Duplicate Conformers*, https://github.com/TheKjaergaardGroup/Removal-of-Duplicate-Conformers.

39. Werner, H.-J., Knowles, P. J., Knizia, G., Manby, F. R., Schütz, M., Celani, P., Györffy, W., Kats, D., Korona, T., Lindh, R., Mitrushenkov, A., Rauhut, G., Shamasundar, K. R., Adler, T. B., Amos, R. D., Bernhardsson, A., Berning, A., Cooper, D. L., Deegan, M. J. O., Dobbyn, A. J., Eckert, F., Goll, R., Hampel, C., Hesselmann, A., Hetzer, G., Hrenar, T., Jansen, G., Köppl, C., Liu, Y., Lloyd, A. W., Mata, R. A., May, A. J., McNicholas, S. J., Meyer, W., Mura, M. E., Nicklass, A., O'Neill, D. P., Palmieri, P., Peng, D., Pflüger, K., Pitzer, R., Reiher, M., Shiozaki, T., Stoll, H., Stone, A. J., Tarroni, R., Thorsteinsson, T., and Wang *MOLPRO, version 2015.1, a package of ab initio programs*, 2015.

40. Møller, K. H.; Bates, K. H.; Kjaergaard, H. G., The Importance of Peroxy Radical Hydrogen-Shift Reactions in Atmospheric Isoprene Oxidation. *J. Phys. Chem. A* **2019,** *123* (4), 920-932.

41. Eckart, C., The Penetration of a Potential Barrier by Electrons. *Physical Review* **1930,** *35* (11), 1303-1309.

42. Kurtén, T.; Rissanen, M. P.; Mackeprang, K.; Thornton, J. A.; Hyttinen, N.; Jørgensen, S.; Ehn, M.; Kjaergaard, H. G., Computational Study of Hydrogen Shifts and Ring-Opening Mechanisms in α-Pinene Ozonolysis Products. *J. Phys. Chem. A* **2015,** *119* (46), 11366-11375.

43. D'Ambro, E. L.; Møller, K. H.; Lopez-Hilfiker, F. D.; Schobesberger, S.; Liu, J. M.; Shilling, J. E.; Lee, B.; Kjaergaard, H. G.; Thornton, J. A., Isomerization of Second-Generation Isoprene Peroxy Radicals: Epoxide Formation and Implications for Secondary Organic Aerosol Yields. *Environ. Sci. Technol.* **2017,** *51* (9), 4978-4987.

44. Ehn, M.; Thornton, J. A.; Kleist, E.; Sipilä, M.; Junninen, H.; Pullinen, I.; Springer, M.; Rubach, F.; Tillmann, R.; Lee, B.; Lopez-Hilfiker, F.; Andres, S.; Acir, I.-H.; Rissanen, M.; Jokinen, T.; Schobesberger, S.; Kangasluoma, J.; Kontkanen, J.; Nieminen, T.; Kurtén, T.; Nielsen, L. B.; Jørgensen, S.; Kjaergaard, H. G.; Canagaratna, M.; Maso, M. D.; Berndt, T.; Petäjä, T.; Wahner, A.; Kerminen, V.-M.; Kulmala, M.; Worsnop, D. R.; Wildt, J.; Mentel, T. F., A large source of low-volatility secondary organic aerosol. *Nature* **2014,** *506* (7489), 476-479.

45. Draper, D. C.; Myllys, N.; Hyttinen, N.; Møller, K. H.; Kjaergaard, H. G.; Fry, J. L.; Smith, J. N.; Kurtén, T., Formation of Highly Oxidized Molecules from NO3 Radical Initiated Oxidation of Δ-3-Carene: A Mechanistic Study. *ACS Earth and Space Chemistry* **2019,** *3* (8), 1460-1470.

46. Lopez-Hilfiker, F. D.; Mohr, C.; Ehn, M.; Rubach, F.; Kleist, E.; Wildt, J.; Mentel, T. F.; Carrasquillo, A. J.; Daumit, K. E.; Hunter, J. F.; Kroll, J. H.; Worsnop, D. R.; Thornton, J. A., Phase partitioning and volatility of secondary organic aerosol components formed from α-pinene ozonolysis and OH oxidation: the importance of accretion products and other low volatility compounds. *Atmos. Chem. Phys.* **2015,** *15* (14), 7765-7776.

47. Schobesberger, S.; D'Ambro, E. L.; Lopez-Hilfiker, F. D.; Mohr, C.; Thornton, J. A., A model framework to retrieve thermodynamic and kinetic properties of organic aerosol from composition-resolved thermal desorption measurements. *Atmos. Chem. Phys.* **2018,** *18* (20), 14757-14785.

48. Lopez-Hilfiker, F. D.; Mohr, C.; D'Ambro, E. L.; Lutz, A.; Riedel, T. P.; Gaston, C. J.; Iyer, S.; Zhang, Z.; Gold, A.; Surratt, J. D.; Lee, B. H.; Kurten, T.; Hu, W. W.; Jimenez, J.; Hallquist, M.; Thornton, J. A., Molecular composition and volatility of organic aerosol in the southeastern US: Implications for IEPOX derived SOA. *Environ. Sci. Technol.* **2016,** *50* (5), 2200-2209.

49. Thomsen, D.; Elm, J.; Rosati, B.; Skønager, J. T.; Bilde, M.; Glasius, M., Large Discrepancy in the Formation of Secondary Organic Aerosols from Structurally Similar Monoterpenes. *ACS Earth and Space Chemistry* **2021,** *5* (3), 632-644.
50. Colville, C. J.; Griffin, R. J., The roles of individual oxidants in secondary organic aerosol formation from Δ3-carene: 1. gas-phase chemical mechanism. *Atmospheric Environment* **2004,** *38* (24), 4001-4012.
51. Baptista, L.; Fernandes Francisco, L.; Dias, J. F.; da Silva, E. C.; Ferreira dos Santos, C. V.; Gil de Mendonça, F. S.; Arbilla, G., Theoretical study of Δ-3-(+)-carene oxidation. *Physical Chemistry Chemical Physics* **2014,** *16* (36), 19376-19385.
52. BIOVIA *COSMOtherm*, Dassault Systèmes: 2021.
53. Kurtén, T.; Hyttinen, N.; D'Ambro, E. L.; Thornton, J.; Prisle, N. L., Estimating the saturation vapor pressures of isoprene oxidation products C5H12O6 and C5H10O6 using COSMO-RS. *Atmos. Chem. Phys.* **2018,** *18* (23), 17589-17600.
54. Kurtén, T.; Møller, K. H.; Nguyen, T. B.; Schwantes, R. H.; Misztal, P. K.; Su, L.; Wennberg, P. O.; Fry, J. L.; Kjaergaard, H. G., Alkoxy Radical Bond Scissions Explain the Anomalously Low Secondary Organic Aerosol and Organonitrate Yields From α-Pinene + NO3. *The Journal of Physical Chemistry Letters* **2017,** *8* (13), 2826-2834.
55. Vereecken, L.; Peeters, J., Decomposition of substituted alkoxy radicals—part I: a generalized structure–activity relationship for reaction barrier heights. *Physical Chemistry Chemical Physics* **2009,** *11* (40), 9062-9074.
56. Vereecken, L.; Peeters, J., A structure–activity relationship for the rate coefficient of H-migration in substituted alkoxy radicals. *Physical Chemistry Chemical Physics* **2010,** *12* (39), 12608-12620.
57. Xu, L.; Møller, K. H.; Crounse, J. D.; Otkjær, R. V.; Kjaergaard, H. G.; Wennberg, P. O., Unimolecular Reactions of Peroxy Radicals Formed in the Oxidation of α-Pinene and β-Pinene by Hydroxyl Radicals. *J. Phys. Chem. A* **2019,** *123* (8), 1661-1674.
58. Park, J.; Jongsma, C. G.; Zhang, R.; North, S. W., OH/OD Initiated Oxidation of Isoprene in the Presence of O2 and NO. *J. Phys. Chem. A* **2004,** *108* (48), 10688-10697.
59. Wu, D.; Bayes, K. D., Rate constants for the reactions of isobutyl, neopentyl, cyclopentyl, and cyclohexyl radicals with molecular oxygen. *Int. J. Chem. Kinet.* **1986,** *18* (5), 547-554.
60. Chacon-Madrid, H. J.; Henry, K. M.; Donahue, N. M., Photo-oxidation of pinonaldehyde at low NO_x: from chemistry to organic aerosol formation. *Atmos. Chem. Phys.* **2013,** *13* (6), 3227-3236.
61. Chacon-Madrid, H. J.; Presto, A. A.; Donahue, N. M., Functionalization vs. fragmentation: n-aldehyde oxidation mechanisms and secondary organic aerosol formation. *Physical Chemistry Chemical Physics* **2010,** *12* (42), 13975-13982.
62. Yee, L. D.; Kautzman, K. E.; Loza, C. L.; Schilling, K. A.; Coggon, M. M.; Chhabra, P. S.; Chan, M. N.; Chan, A. W. H.; Hersey, S. P.; Crounse, J. D.; Wennberg, P. O.; Flagan, R. C.; Seinfeld, J. H., Secondary organic aerosol formation from biomass burning intermediates: phenol and methoxyphenols. *Atmos. Chem. Phys.* **2013,** *13* (16), 8019-8043.
63. Donahue, N. M.; Henry, K. M.; Mentel, T. F.; Kiendler-Scharr, A.; Spindler, C.; Bohn, B.; Brauers, T.; Dorn, H. P.; Fuchs, H.; Tillmann, R.; Wahner, A.; Saathoff, H.; Naumann, K.-H.; Möhler, O.; Leisner, T.; Müller, L.; Reinnig, M.-C.; Hoffmann, T.; Salo, K.; Hallquist, M.; Frosch, M.; Bilde, M.; Tritscher, T.; Barmet, P.; Praplan, A. P.; DeCarlo, P. F.; Dommen, J.; Prévôt, A. S. H.; Baltensperger, U., Aging of biogenic secondary organic aerosol via gas-phase OH radical reactions. *Proceedings of the National Academy of Sciences* **2012,** *109* (34), 13503-13508.
64. Chhabra, P. S.; Ng, N. L.; Canagaratna, M. R.; Corrigan, A. L.; Russell, L. M.; Worsnop, D. R.; Flagan, R. C.; Seinfeld, J. H., Elemental composition and oxidation of chamber organic aerosol. *Atmos. Chem. Phys.* **2011,** *11* (17), 8827-8845.

65. Henry, K. M.; Donahue, N. M., Photochemical Aging of α-Pinene Secondary Organic Aerosol: Effects of OH Radical Sources and Photolysis. *J. Phys. Chem. A* **2012,** *116* (24), 5932-5940.
66. Garmash, O.; Rissanen, M. P.; Pullinen, I.; Schmitt, S.; Kausiala, O.; Tillmann, R.; Zhao, D.; Percival, C.; Bannan, T. J.; Priestley, M.; Hallquist, Å. M.; Kleist, E.; Kiendler-Scharr, A.; Hallquist, M.; Berndt, T.; McFiggans, G.; Wildt, J.; Mentel, T. F.; Ehn, M., Multi-generation OH oxidation as a source for highly oxygenated organic molecules from aromatics. *Atmos. Chem. Phys.* **2020,** *20* (1), 515-537.
67. Atkinson, R.; Arey, J., Atmospheric Degradation of Volatile Organic Compounds. *Chemical Reviews* **2003,** *103* (12), 4605-4638.
68. Kwok, E. S. C.; Atkinson, R., Estimation of hydroxyl radical reaction rate constants for gas-phase organic compounds using a structure-reactivity relationship: An update. *Atmospheric Environment* **1995,** *29* (14), 1685-1695.
69. Hasson, A. S.; Kuwata, K. T.; Arroyo, M. C.; Petersen, E. B., Theoretical studies of the reaction of hydroperoxy radicals (HO2) with ethyl peroxy (CH3CH2O2), acetyl peroxy (CH3C(O)O2), and acetonyl peroxy (CH3C(O)CH2O2) radicals. *Journal of Photochemistry and Photobiology A: Chemistry* **2005,** *176* (1), 218-230.
70. Groß, C. B. M.; Dillon, T. J.; Schuster, G.; Lelieveld, J.; Crowley, J. N., Direct Kinetic Study of OH and O3 Formation in the Reaction of CH3C(O)O2 with HO2. *J. Phys. Chem. A* **2014,** *118* (6), 974-985.
71. Iyer, S.; Reiman, H.; Møller, K. H.; Rissanen, M. P.; Kjaergaard, H. G.; Kurtén, T., Computational Investigation of RO2 + HO2 and RO2 + RO2 Reactions of Monoterpene Derived First-Generation Peroxy Radicals Leading to Radical Recycling. *J. Phys. Chem. A* **2018,** *122* (49), 9542-9552.
72. Yang, L. H.; Takeuchi, M.; Chen, Y.; Ng, N. L., Characterization of thermal decomposition of oxygenated organic compounds in FIGAERO-CIMS. *Aerosol Sci. Technol.* **2021**, 1-22.
73. Vereecken, L.; Peeters, J., Nontraditional (Per)oxy Ring-Closure Paths in the Atmospheric Oxidation of Isoprene and Monoterpenes. *J. Phys. Chem. A* **2004,** *108* (24), 5197-5204.
74. Compernolle, S.; Ceulemans, K.; Muller, J. F., EVAPORATION: a new vapour pressure estimation method for organic molecules including non-additivity and intramolecular interactions. *Atmos. Chem. Phys.* **2011,** *11* (18), 9431-9450.
75. Roldin, P.; Ehn, M.; Kurtén, T.; Olenius, T.; Rissanen, M. P.; Sarnela, N.; Elm, J.; Rantala, P.; Hao, L.; Hyttinen, N.; Heikkinen, L.; Worsnop, D. R.; Pichelstorfer, L.; Xavier, C.; Clusius, P.; Öström, E.; Petäjä, T.; Kulmala, M.; Vehkamäki, H.; Virtanen, A.; Riipinen, I.; Boy, M., The role of highly oxygenated organic molecules in the Boreal aerosol-cloud-climate system. *Nature Communications* **2019,** *10* (1), 4370.

818 **For Table of Contents Only**

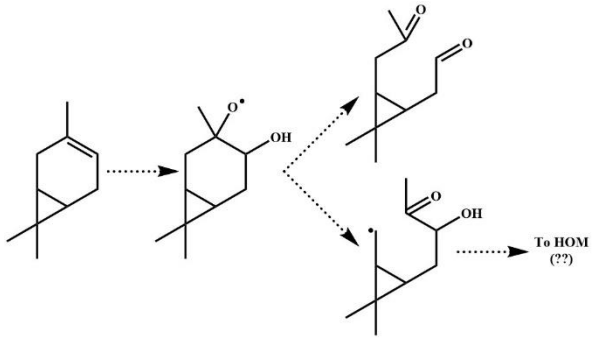

819

820